Photoemission and Photon Screening in Layered Crystals

A. Bödicker, A. Leventi-Peetz, and W. Schattke

Institut für Theoretische Physik, Universität Kiel
Leibnizstraße 15, D-24118 Kiel, Germany

Previously it was shown that above the plasma frequency the photoemission intensities crucially depend on the screening of the photon field by virtual plasmon excitation at the surface of the solid. This, usually being neglected in the most precise calculations within the one-step model, led to a considerable improvement of the agreement between theory and experiment. Here, we regard as an additional effect the bulk microscopic screening by taking into account the possibility of local fields. Because the discrepancies between the theory without screening corrections and experiment extend to frequencies below the plasma frequency, we consider these frequencies here. The outlined procedure is not limited to this range. We report on calculations of the full dielectric function and the one-step photoemission spectra for $TiSe_2$, a layered material where those effects are expected to become transparent.

1 INTRODUCTION

Actual theoretical investigations on valence band photoemission in the vacuum ultraviolet (VUV) photon range rely on the highly accurate one-step model to quantitatively determine energy distribution spectra. [1, 2] The high precision of this model originates from the full consideration of the golden rule incorporating excitation, transport through the solid, and emission into the detector as an integral process. However, that accuracy can be strongly affected if the light wave undergoes screening. On one hand, this is usually neglected owing to the long wavelength of the VUV radiation, on the other, one has to expect local response fields just in this frequency regime, because it usually covers the plasma frequency of the solid. In a systematic expansion this screening arises as a natural part.[3] It is the aim of this paper, to demonstrate quantitatively the importance of those fields and its effect on the photocurrent. As prototype we have chosen a compound from the class of layered transition metal dichalcogenides, $TiSe_2$. The band structure for momenta perpendicular to the layers (Γ–A) has been experimentally investigated in detail by angle resolved direct and inverse photoemission. [4, 5] Similar phenomena have been already suspected as being responsible for strong specific deviations observed between experimental and theoretical photoemission spectra in these materials. [6, 7]

2 DIELECTRIC FUNCTION

In this section the method of calculation and the results for the dielectric function are presented. This quantity provides the screened vector potential for the golden rule formula of photoemission by the relation

$$\mathbf{A}^{scr}(\mathbf{r};\omega) = \sum_{\mathbf{G}} e^{i\mathbf{G}\mathbf{r}} \boldsymbol{\epsilon}^{-1}(\mathbf{G},\mathbf{0};\omega)\mathbf{A}^{phot}. \quad (1)$$

The sum runs over the vectors of the reciprocal lattice. The z-axis is chosen along the surface normal pointing into the vacuum. It coincides with the threefold symmetry axis perpendicular to the natural cleavage plane of this crystal which belongs to space group $P\overline{3}m1$. It turns out that the observed resonant enhancement by the local fields appears in the ϵ_{zz}^{-1} and not in the ϵ_{xx}^{-1} or ϵ_{yy}^{-1} tensor components. Therefore and because of

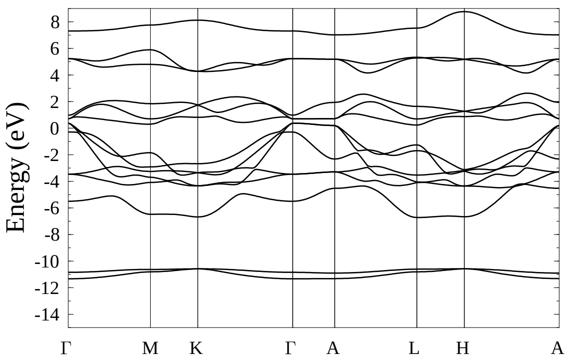

Figure 1: Tight-binding bandstructure used for calculating the dielectric function. The lowest two bands with Se-s character are followed by six Se-p bands with increasing mixing of Ti-d orbitals. Above the Fermi energy, 0 eV, a Ti-s band appears at the top of the plot besides the Ti-d bands below. The normal emission photocurrent derives from the $\Gamma-$A momentum direction.

the long wavelength of the incident radiation, we may consider in the following the scalar response only. Equation 1 then involves the longitudinal dielectric function ϵ_l and simplifies to

$$\begin{aligned} A_z^{scr}(z) \; &= \; A_z^{phot}(\epsilon_l^{-1}(\eta\mathbf{e}_z,\eta\mathbf{e}_z;\omega) \\ &\quad + \sum_{G_z\neq 0} e^{iG_z z} G_z \epsilon_l^{-1}(G_z\mathbf{e}_z,\eta\mathbf{e}_z;\omega)/\eta) \end{aligned} \quad (2)$$

The above equation is understood in the limit $\eta \to 0$, with $\mathbf{e}_z$ denoting the unit vector along the z-axis. It is summed only over reciprocal lattice vectors parallel to the layer normal, because these components dominate when the local field effect evolves. The influence of the surface is considered classically by the continuity conditions for the scalar fields. Refraction is neglected in this long wavelength limit. In a model calculation the non-classical surface response has previously been shown not to contribute significantly to the photocurrent. [9]

The dielectric function is determined via a tight binding basis set for its full dependence on frequency, on momentum and on reciprocal lattice vectors. The wavefunctions are optimized to give a reasonable approximation of an ab initio bandstructure which was previously obtained from an extended LAPW-calculation. [7] The applied bandstructure is shown in figure 1. With these wavefunctions and energies the polarizability is determined within the random phase ap-

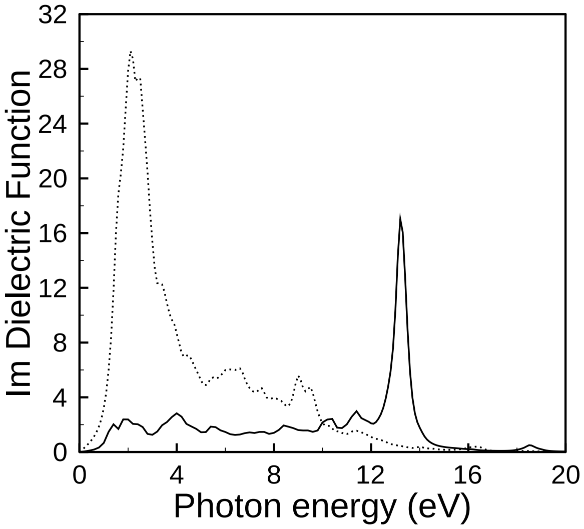

Figure 2: Imaginary part of the macroscopic dielectric constant $(\epsilon_{ii}^{-1}(\mathbf{0},\mathbf{0},\omega))^{-1}$ for $i=z$, solid, and $i=x$, dashed. Note the local field effects in the z-component at 13.5 and 18.5 eV. The plasma frequency arises from the real part at 19.6 eV.

proximation (RPA) to yield the dielectric function. The matrix inversion with respect to the reciprocal lattice vectors is performed using the factorization property of a degenerate integral kernel. The calculation closely follows the procedure outlined in Leventi et al. [7].

First, the macroscopic frequency dependent dielectric constants, i.e. $(\epsilon_{ii}^{-1}(\mathbf{0},\mathbf{0}))^{-1}$ for $i=x,z$, were obtained. The corresponding RPA results are displayed for the imaginary part in figure 2. A significant local field effect is observed in the z-component at about 13.5 eV and a smaller one at about 18.5 eV whereas the x-component does not show much structure within this energy range. The effect arises through the matrix inversion by some nondiagonal elements with reciprocal lattice vectors normal to the layer which are dominant over the diagonal elements in approaching the plasma frequency.

In figure 3 those matrix elements of the inverse dielectric function which contribute to equation 2 are plotted for the lowest two layer perpendicular reciprocal lattice vectors. The next following element is smaller by an order of magnitude than the preceeding one. They are proportional to the respective Fourier components of the local field along the z-axis. Both anomalies detected

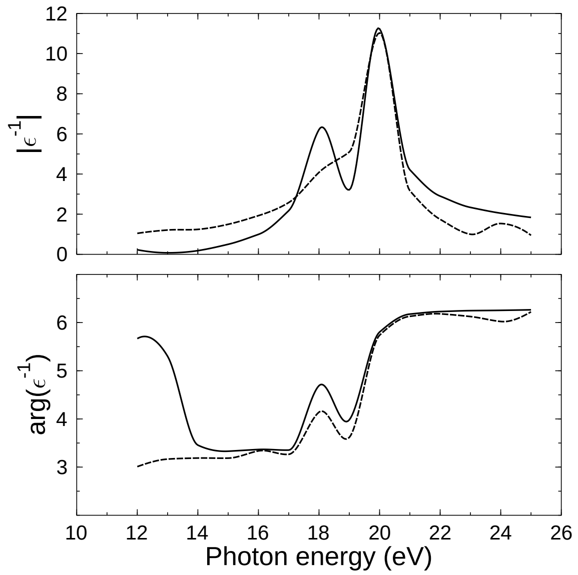

Figure 3: Modulus (upper panel) and phase (lower panel) of the inverse dielectric function components $\epsilon_{zz}^{-1}(\mathbf{0},\mathbf{0};\omega)$ and $\epsilon_{zz}^{-1}(\frac{2\pi}{c}\mathbf{e}_z,\mathbf{0};\omega)$ plotted vs. frequency as solid and broken line, respectively. The modulus shown by the broken line has been augmented by a factor of 5.

in the macroscopic dielectric constant are seen to be present also in these components, but in a differing shape. Close to the plasma frequency the local field contribution appears as a faint peak in the macroscopic dielectric constant, s. figure 2, whereas the field itself, plotted here, gains a considerable magnitude around 19 eV. Both components are roughly in phase. Opposed to this behavior, the large peak at 13.5 eV in figure 2 is not accompanied by a significant change in the local field, but by a large phase difference between both components.

3 PHOTOEMISSION

The photoemission calculation within the one-step model starts with the golden rule formula which is written for our purpose in the form

$$I \propto \quad Im \sum_{i,j} \; < \Phi^{\star}_{LD}(E,\mathbf{k}_{\|}) \mid \mathbf{O} \mid \psi_i > \cdot\, G_{i,j}(E-\hbar\omega,\mathbf{k}_{\|}) \cdot < \psi_j \mid \mathbf{O} \mid \Phi^{\star}_{LD}(E,\mathbf{k}_{\|}) > \qquad (3)$$

with $\mathbf{O} = \mathbf{p}\cdot\mathbf{A} + \mathbf{A}\cdot\mathbf{p}$ and $G_{i,j}(E, \mathbf{k}_{\|})$, as the halfspace Greens function of the valence states in a layer orbital LCAO basis i, j.[2] The valence band structure has been slightly improved beyond that used in the calculation of the dielectric function, because for the latter the formalism required restrictions with respect to the parametrization of the overlap integrals. This yields the peak positions in the photoemission spectra at the appropriate positions. It would not have influenced the local field effects due to the essentially different energy ranges. The final state corresponds to $\mid \Phi^{\star}_{LD}(E, \mathbf{k}_{\|}) >$, an inverse LEED state for the detected electron. It is constructed from the complex bandstructure of a pseudopotential representation inside the crystal. The surface is terminated by a step like solid–vacuum barrier potential. The wavefunction of the final state results from matching the bulk to the vacuum solutions. The matrix elements are decomposed into halfspace Fourier transforms of the initial state atomic orbitals.

In figure 4 a series of normal emission spectra is shown with both, the bare external vector potential and that screened along the lines of the preceeding section. The strong deviations between both series are overwhelming in the shown photon range. They emerge essentially from p_z emissions which disperse along Γ–A and appear e.g. at 1.6 and 5.2 eV binding energy in the 19 eV photon energy spectrum. A large amount of relative intensity is carried by these peaks in comparison with the nondispersive structures at 0 and 3 eV binding energy, the latter deriving from inplane bonding orbitals. The effect is strongest close to the plasma frequency where according to figure 2 the upper local field effect arises. It is suppressed below, especially near the large peak of the macroscopic dielectric constant at 13.5 eV. These effects are not unpredictable. On one hand, the case of layered crystals surely accentuates the anomaly because of anisotropy. On the other hand, those local fields occur in a limited frequency range around the plasma frequency. If, in addition, the local fields couple to a special emission, as e.g. to the clearly isolated dispersive peaks of the p_z orbitals in this case, then the conditions are very advantageous to identify the influences considered here. In the opposite case these effects could be hidden, e.g. by orbital mixing, so that the causes for a disagreement between experiment and a calculation within the familiar one-step model are less obvious.

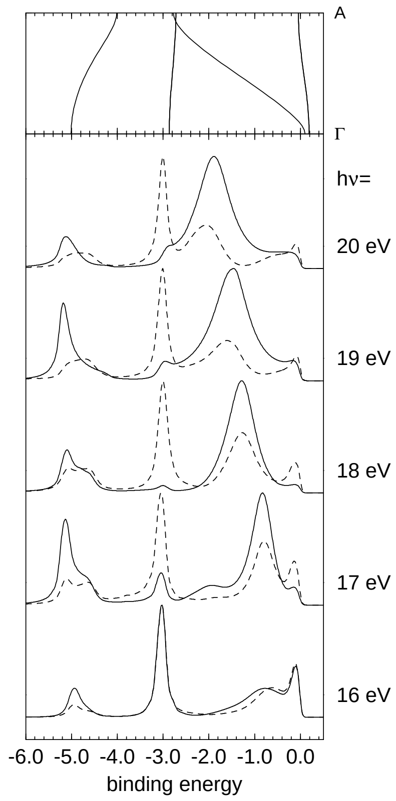

Figure 4: Photocurrent vs. initial state energy of normal emission spectra for photon frequencies as indicated at the curves with incidence angle of 45°. The screening of the photon yields the solid lines as opposed to the unscreened result depicted by the broken lines. The upper panel shows the respective part of the bandstructure.

4 CONCLUSIONS

The microscopic screening of the incident light in photoemission may attain anomalous behavior far from classical predictions and establish extreme changes in the spectra. They are intimately connected with the local fields near the plasma frequency. Together with the plasmon screening above the plasma frequency [8] a considerable interval around this frequency is thus subject to a strong dielectric response. It should be expected that these dielectric effects appear also in other covalently bond materials like e.g. semiconductors.

This work was supported by the Deutsche Forschungsgemeinschaft under contract no. Scha 360/7-1.

References

[1] S.V. Halilov, E. Tamura, H. Gollisch, D. Meinert, and R. Feder, J. Phys. Condens. Matter 5 (1993) 3859.

[2] J. Henk, W. Schattke, H. Carstensen, R. Manzke, M. Skibowski, Phys. Rev. B 47 (1993) 2251.

[3] C.-O. Almbladh, Physica Scripta 32 (1985) 341.

[4] O. Anderson, R. Manzke, M. Skibowski, Phys. Rev. Lett. 55 (1985) 2188.

[5] D. Straub, M. Skibowski, F.J. Himpsel, W. Drube, Phys. Rev. B 31 (1985) 8254.

[6] E. Pehlke, W. Schattke, O. Anderson, R. Manzke, M.Skibowski, Phys. Rev. B 41 (1990) 2982.

[7] A. Leventi-Peetz, E.E. Krasovskii, W. Schattke, Phys. Rev. B 51 (1995) 17965.

[8] D. Samuelsen, E. Pehlke, W. Schattke, O. Anderson, R. Manzke, M. Skibowski, Phys. Rev. Letters 68 (1992) 522.

[9] D. Samuelsen, W. Schattke, Surface Sci. **327**, 379 (1995).